Journal of Hunan University

(Natural Sciences)

Vol. 52 No. 7

July 2025

Available online at

https://jonuns.com

Open Access Article

https://doi.org/10.55463/issn.1674-2974.52.7.6

Experimental Study on the Behavior of Spiral Grouped-Piles Installed in Sand Soil under Lateral Cyclic Loading

Mahmoud F. Awad-Allah[1*], Ryohei Ishikura[2], Adel Alowaisy[2], Takahiro Kurokawa[3]

[1]Department of Civil Engineering, National Research Center, Cairo, Egypt

[2]Department of Civil Engineering, Kyushu University, Fukuoka, Japan

[3]Hinode Holdings Co, Ltd, Hinode Global Innovation Center, Saga, Japan

* Corresponding author: mf.awad-alla@nrc.sci.eg, mahmoud_fawzi@hotmail.com

Article History:

Received: June 4, 2025
Revised: July 2, 2025
Accepted: July 17, 2025
Published: August 30, 2025

Abstract:
Background: Spiral piles are a promising foundation solution for onshore renewable-energy structures; however, their lateral cyclic performance, particularly in grouped configurations, remains insufficiently understood. This study investigates the influence of key design and loading parameters on the behavior and stability of steel spiral pile groups under lateral cyclic loading.
Methods: A 1-g physical modeling program was conducted in medium-dense sand (relative density, $D_r \approx 50\%$). Two group arrangements (2×1 and 1×2) were tested with three slenderness ratios (L/B = 9, 13.5, 18) and three batter angles ($\theta = 0°, 15°, 30°$). Reversed (two-way), displacement-controlled lateral cyclic loading was applied for up to N = 200 cycles across a range of loading frequencies (f). The response was evaluated using normalized load–displacement curves, stiffness degradation trends, and accumulated residual displacements.
Results: The tests reveal systematic dependencies of lateral performance on the number of cycles (N), frequency (f), slenderness ratio (L/B), batter angle (θ), and group arrangement.

Increasing N and f amplifies stiffness degradation and residual drift. More slender piles exhibit greater lateral compliance, while battered groups (15°–30°) demonstrate reduced deformation and higher normalized lateral resistance compared to vertical groups, depending on the arrangement and loading direction. Group layout (2×1 vs. 1×2) significantly influences load sharing and failure mechanisms, resulting in distinct normalized response envelopes.

Conclusions: The experimental results identify the primary geometric and loading factors governing the stability of spiral pile groups and provide normalized response data to support preliminary design and parameter selection. These findings contribute to the broader adoption of steel spiral pile foundations in onshore renewable-energy infrastructure, where reliable performance under lateral cyclic loads is critical.

Keywords: Spiral pile; grouped-piles; 1-g model; sand; soil rocking; cyclic loading.

砂土中螺旋群桩横向循环荷载作用下的试验研究

摘要：

背景：螺旋桩是陆上可再生能源结构的一种有前景的基础解决方案；然而，其横向循环性能，尤其是在组合配置中，仍未得到充分了解。本研究探讨了关键设计和荷载参数对钢螺旋桩群在横向循环荷载作用下性能和稳定性的影响。

方法：在中密砂土（相对密度，$D_r \approx 50\%$）中进行了 1g 物理建模程序。对两种组合布置（2×1 和 1×2）进行了试验，试验中采用了三种长细比（L/B = 9、13.5、18）和三种倾斜角（θ = 0°、15°、30°）。在一系列荷载频率（f）下施加反向（双向）、位移控制的横向循环荷载，最多 N = 200 次循环。使用归一化荷载-位移曲线、刚度衰减趋势和累积残余位移来评估响应。

结果：试验揭示了横向性能与循环次数（N）、频率（f）、长细比（L/B）、倾斜角（θ）和桩群布置之间的系统依赖关系。增加 N 和 f 会加剧刚度退化和残余漂移。较细长的桩表现出更高的横向柔度，而倾斜桩群（15°–30°）与垂直桩群相比，变形更小，标准化横向阻力更高，具体取决于布置和荷载方向。桩群布局（2×1 vs. 1×2）显著影响荷载分配和失效机制，从而产生不同的标准化响应包络线。

结论：试验结果确定了控制螺旋桩群稳定性的主要几何和荷载因素，并提供了标准化响应数据以支持初步设计和参数选择。这些发现有助于钢螺旋桩基础在陆上可再生能源基础设施中的更广泛应用，在这些基础设施中，横向循环荷载下的可靠性能至关重要。

关键词：螺旋桩；群桩；1-g 模型；砂土；土体摇动；循环荷载。

1. Introduction

The foundations of small wind turbine and solar panel structures in onshore renewable energy farms are subjected to multiple load types, including cyclic, static gravitational, and dynamic lateral loads induced by environmental forces. In wind turbine structures, the primary external excitations are:

(A) environmental dynamic loads from wind and ground vibrations;

(B) rotational frequency (1P); and

(C) blade passing frequency (3P) [1].

In contrast, solar panel structures are primarily subjected to cyclic lateral and uplift loads due to wind gusts and fluctuating pressure differentials across the panel surface [2].

In recent years, an innovative foundation system has been developed for supporting structures in renewable energy installations: the steel spiral pile. This foundation consists of a high-strength steel shaft with one or more helical plates welded in a continuous spiral configuration, as illustrated in Figure 1 [3]. Research by [4] indicates that the optimal ratio of helix pitch (p) to plate width (B) is 4.5, which maximizes load transfer efficiency and installation performance.

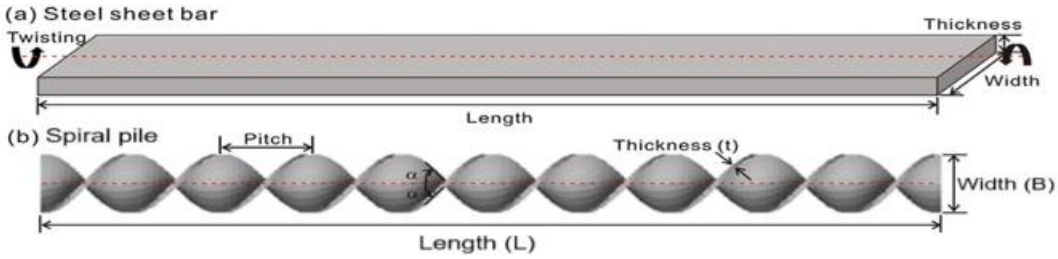

Figure 1. Typical configuration and manufacturing concept of the innovative spiral pile. (Source:[3])

Due to their simple installation, recyclability, and high axial load-bearing capacity, spiral piles have been increasingly adopted as foundation solutions for a variety of geotechnical applications in Japan, including solar photovoltaic panels, wind turbines, guide rails, pedestrian guardrails, traffic and road signs, and even rock bolting systems [3], [5-6].

Spiral piles are installed by screwing them into the ground through the application of torque at the pile head, often combined with a compressive (crowd) force. Importantly, they can be removed through reverse rotation, enabling reuse and minimizing ground disturbance [7]. While spiral piles exhibit high axial resistance, they possess lower bending rigidity compared to steel pipe piles of equivalent diameter and wall thickness [8].

Cyclic loading on pile foundations is typically characterized by four key parameters:

(1) maximum lateral load (H_{max}),

(2) number of load cycles (N),

(3) loading frequency (f, defined as the inverse of the time period, 1/t), and

(4) maximum lateral displacement (y_{max}).

As noted by [9], two-way lateral cyclic loading can serve as a simplified representation of dynamic environmental loads, such as those from wind or wave action, without accounting for inertial or damping effects.

Furthermore, logarithmic and exponential expressions were introduced by [11] based on the concept of a degradation factor to model the cyclic degradation of pile-soil systems. In addition, cyclic triaxial tests were used by [12, 13] in laboratory studies to investigate the mechanical degradation of pile-soil interaction under repeated loading. Small-scale (1-g) physical modeling tests were performed on pipe piles subjected to two-way lateral cyclic loading in partially saturated sandy soil [14]. A three-dimensional finite element analysis was implemented by [15] to simulate the behavior of large-scale monopile foundations under cyclic lateral loads. The bearing capacity of spiral piles was investigated and characterized using an elastoplastic finite element method (FEM), providing insights into their nonlinear load-transfer mechanisms [16].

Table 1 summarizes the most well-known mathematical models and formulas for modeling of lateral cyclic loading on piles documented in the literature and proposed by several researchers. [10] carried out comprehensive laboratory and field lateral cyclic pile load tests.

Table 1. Mathematical models and formulas for the lateral cyclic loading response documented in the literature. (Source: compiled by the authors)

Equation	Researcher (Reference)
$p = Ap_u\, tanh\left(\frac{K_h.z}{Ap_u}y\right)$	[21]
$p_N = p_1 N^{(\chi-1)m}$ $y_N = y_1 N^{\chi m}$	[10]
$y_N = y_1 N^{0.136}$	[12]
$y_N = y(1 + C_N \ln N)$	[13]
$\frac{\varepsilon_N}{\varepsilon_1} = 1 + \chi \ln(N)$	[11]
$\frac{E_{sN}}{E_{s1}} = \frac{\varepsilon^a_{cp,N=1}}{\varepsilon^a_{cp,N}} = N^{-b_1 (X_C)^{b_2}}$	[15]
$K_h = \chi n_h z$	[22]
$K_{hN} = K_{h1} N^{-\zeta}$	[10]
$K_N = K_1 + A_K\, ln(N)$	[23]

Note:

p = lateral soil resistance;

p_u = static ultimate soil resistance;

p_1 and p_N= soil resistance at 1st and at Nth cycles, respectively;

K_h = horizontal modulus of subgrade reaction;

K_1 and K_N= pile lateral stiffness at the 1st cycle and at the Nth cycles, respectively;

K_{h1} and K_{hN}= horizontal modulus of subgrade reaction at the 1st and at the Nth cycles, respectively;

y = lateral soil displacement;

y_1 and y_N= lateral soil displacement at the 1st and at the Nth cycles, respectively;

z = distance from the soil surface;

ε_1 and ε_N = lateral soil strains at the 1st and at the Nth cycles, respectively;

$\varepsilon^a_{cp,1}$ and $\varepsilon^a_{cp,N}$ = axial plastic strains at the 1st and at the Nth cycles, respectively;

X_c = characteristic cyclic stress ratio;

E_{s1} and E_{sN}= soil stiffness (Young's modulus) at the 1st and at the Nth cycles, respectively;

m = a dimensionless factor;

A = a reduction factor to be considered for both monotonic loading (A=0.9) and cyclic loading (A=3-0.8z/B);

B = pile diameter;

N= number of load cycles;

b_1 and b_2 = regression parameters obtained from cyclic triaxial test results;
ζ and χ = degradation factors, and
C_N is a factor equal to 0.2 for sand.

A formula was proposed by [2] for estimating the bearing capacity of both straight and battered spiral piles under combined loading conditions, including vertical, lateral, and moment loads. Furthermore, the in-soil behavior of eco-spiral piles was investigated by [3], focusing on the effects of twisting angle and the ratio of borehole diameter to pile width, using three-dimensional numerical simulations in FLAC-3D based on the finite difference method. Most recently, the ultimate load-carrying resistance of toe-wing (Tsubasa) and spiral screw piles were examined to optimize their design and installation procedures [17].

Regarding experimental studies conducted at 1-g scale, several researchers have performed small-scale laboratory model tests on spiral piles installed in sandy soil formations [6], [18-20].

Despite the significant amount of research conducted to describe the design of pile foundations, the use of spiral pile foundations has not received much attention by geotechnical researchers. Moreover, a few experimental and field studies have been reported on the behavior of spiral piles under lateral cyclic loading. Moreover, the literature indicates that all available mathematical models, formulas, and the current theories were proposed for pipe (circular) pile foundations, and the current analysis of spiral pile foundations are still approximate and empirical approaches. Furthermore, they ignored some of the key parameters, including: slenderness of the piles (L/B), loading frequency (f), and number of cycles (N). Accordingly, this research focuses on the investigation of the behavior of spiral grouped piles installed in dry sandy soils when they are subjected to lateral cyclic loading. In addition, the soil-pile interaction response of spiral grouped-pile foundations was investigated under lateral displacement controlled 1-g tests (y = 0.1B, i.e, 50% of the ultimate lateral pile head displacement).

Therefore, to investigate the behavior of spiral pile–soil interaction, an extensive experimental program was conducted using 1-g scale physical models. Within this program, a parametric study was carried out to evaluate the influence of key design and loading variables on lateral pile resistance and the overall stability of spiral pile group foundations supporting onshore renewable energy structures, such as wind turbines and solar panels.

2. Outline of the Experimental Test Setup

2.1 Geotechnical Properties and Ground Soil Preparation

In this study, K-7 silica sand provided by KUMAMOTO-Silica Mining Co. Ltd was adopted as the ground soil material for the laboratory work. Particle size distribution curve for K-7 sand is plotted in Figure 2.

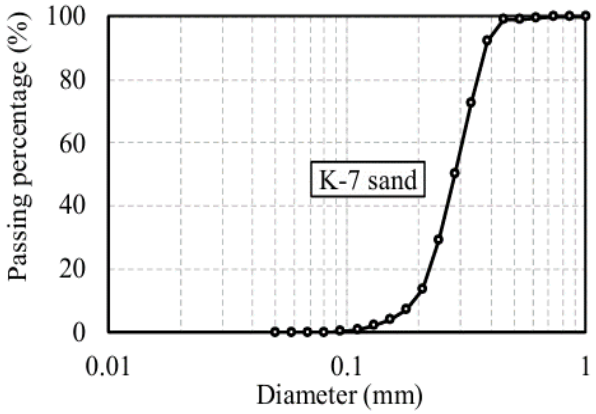

Figure 2. Grain size distribution of the Kumamoto K-7 sand. (Source: developed by the authors)

Moreover, Table 2 gives the geotechnical characteristics of the Kumamoto K-7 sand.

Table 2. Geotechnical properties of the Kumamoto K-7 sand. (Source: compiled by the authors)

Geotechnical parameter	Value
Specific gravity (G_s)	2.63
Maximum dry unit weight (γ_{max})	15.30 kN/m^3
Minimum dry unit weight (γ_{min})	11.67 kN/m^3
Maximum void ratio (e_{max})	1.125
Minimum void ratio (e_{min})	0.719
Uniformity coefficient (U)	1.76
Median diameter (D_{50})	0.18 mm
Effective diameter (D_{10})	0.10 mm
Relative density (D_r)	50%
Internal friction angle (φ)	36.5°
Young's modulus of soil (E_s)	6.50 MPa

Regarding the ground soil setup for testing, the multiple sieving eluviation (MSP) method, which was developed by [24], was adapted for preparing the sand ground inside the testing container. Pluviation, or raining, is a method commonly used to setup sand samples to achieve a certain relative density of sand (D_r). Sand particles are rained down into the testing tank from a designated height through a mesh of sieving. The rate of sand discharge can be controlled by the height of free fall (raining height) and nozzle size. Numerous trials have been conducted to calibrate and adjust the raining height and nozzle size with the required relative density before the beginning of the actual test.

This method has some advantages compared to the standard manual compaction method, including: (1) protecting the installed piles from movement during soil replacement and (2) producing a homogenous testing ground around the pile wall. For all tests conducted, the achieved relative density of K-7 sand is found to vary by 3% (i.e, between 47% and 53%), which is minor variation.

Furthermore, after placing the sand bed ground, a

portable mini-cone penetration test (CPT) was carried as per [25] over the whole depth of the testing tank (60cm). The penetration force of the CPT device was measured while pushing the cone down into the soil at a rate of 1 cm/s. The tip resistance (q_c) is estimated by dividing the penetration force value required to penetrate the soil for a distance of 1 cm by the projected area of the cone (3.14cm^2). Three CPT tests were conducted inside the testing chamber at different locations. Figure 3 shows the results of the penetration resistance (q_c) versus the depth (z). The results indicate that the average cone penetration resistance $(q_c)_{avg}$ is equal to 326 kPa.

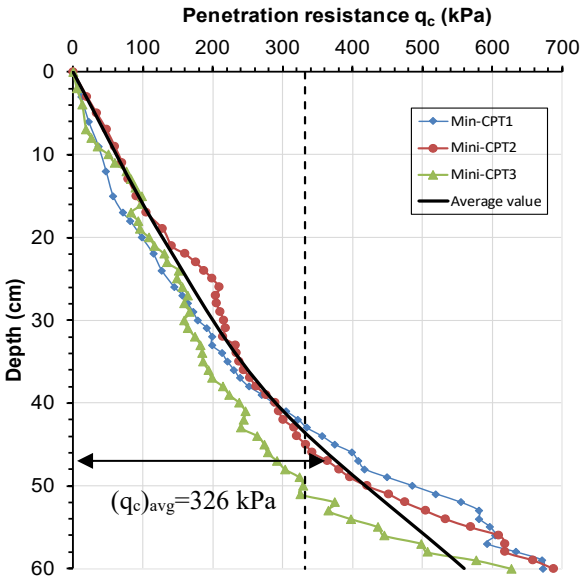

Figure 3. Results of Mini-CPT with depth conducted on K-7 sand. (Source: developed by the authors)

Based on the CPT results, the strength and deformation properties of the ground soil can be estimated using the empirical correlations introduced by [26]. Eqs. (1) and (2) give the empirical formulas for estimating the internal friction angle (φ), and the Young's modulus (Es) of the sand soil.

$$\varphi = 0.21D_r + 26^o \quad (1)$$

$$E_s = 1.45q_c + 6.07 \quad (2)$$

where: D_r = relative density of sand; and q_c= cone penetration resistance in MPa.

2.2 Testing Tank

The dimensions and boundary conditions of the testing tank play a critical role in pile load tests, as they significantly influence the accuracy and reliability of the experimental results. The length-to-height ratio (l/h) of the test container should be designed within the range of 1.5 to 2.0 [27] to minimize scale effects and ensure representative soil behavior. Proper design is essential to reduce the influence of artificial boundaries, such as side walls and the base, on the pile-soil interaction during testing.

Figure 4 shows the section elevation for the testing chamber and the test setup along with the assembly of the lateral loading device, data acquisition system, and measurement equipment. The dimensions of the testing container are 600 mm (length), 300 mm (width), and 600 mm (depth). Moreover, the side walls of the soil chamber were made of a rigid fiberglass material of thickness equal to 5 cm.

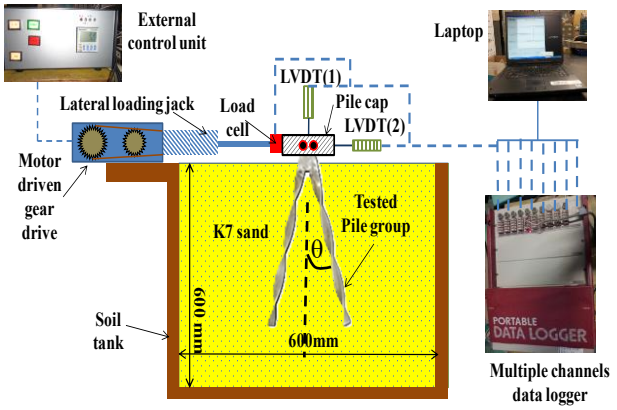

Figure 4. Schematic of the experimental 1-g test setup (Source: [14])

An external control unit was used to regulate the number of applied load cycles (N) and the lateral loading frequency (f). The apparatus for measuring deformations and loads during testing included horizontal and vertical linear variable differential transformers (LVDTs) and a load cell. Lateral cyclic loads were applied at the pile head using a servo-hydraulic actuator connected to the pile cap via steel bolts. To simulate a pinned connection between the pile head and the pile cap, the bolts were tightly fastened to allow rotational freedom while maintaining structural attachment. A detailed description of the testing chamber, loading system, and instrumentation is provided by [14].

2.3 Lateral Load Mechanism

In this testing program, two-way cyclic lateral displacement was imposed on the pile group according to the loading pattern recommended by [28]. This loading regime simulates the dynamic effects of wind forces (based on the Foroya model) over a frequency range of 0.017 Hz to 0.05 Hz.

The cyclic lateral displacement was applied at frequencies ranging from 0.025 Hz to 0.125 Hz, as illustrated in Figure 5. This corresponds to an event period (e.g, storm wind event) between 8 s and 40 s, respectively.

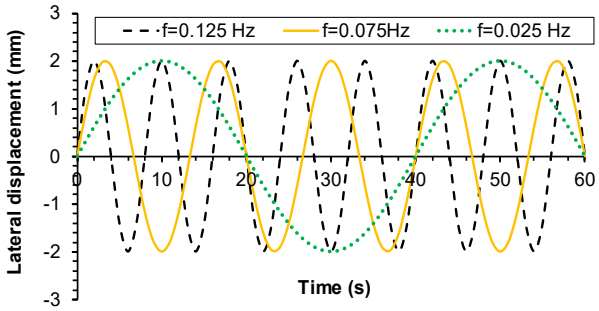

Figure 5. Two-way lateral cyclic displacement for the applied frequency ranges. (Source: developed by the authors)

2.4 Spiral Pile Group Models

The pile models used in this study were fabricated from high-strength steel with the following geometric dimensions: width (B) = 16 mm, wall thickness (t) = 3 mm, and pitch (p) = 72 mm. The mechanical properties of the pile material were as follows: Young's modulus (E) = 200 GPa and yield stress (σ_y) = 443 MPa. Three different batter angles (θ) were employed: 0° (vertical), 15°, and 30°. Additionally, three slenderness ratios (L/B = 9, 13.5, and 18) were investigated, as illustrated in Figure 6.

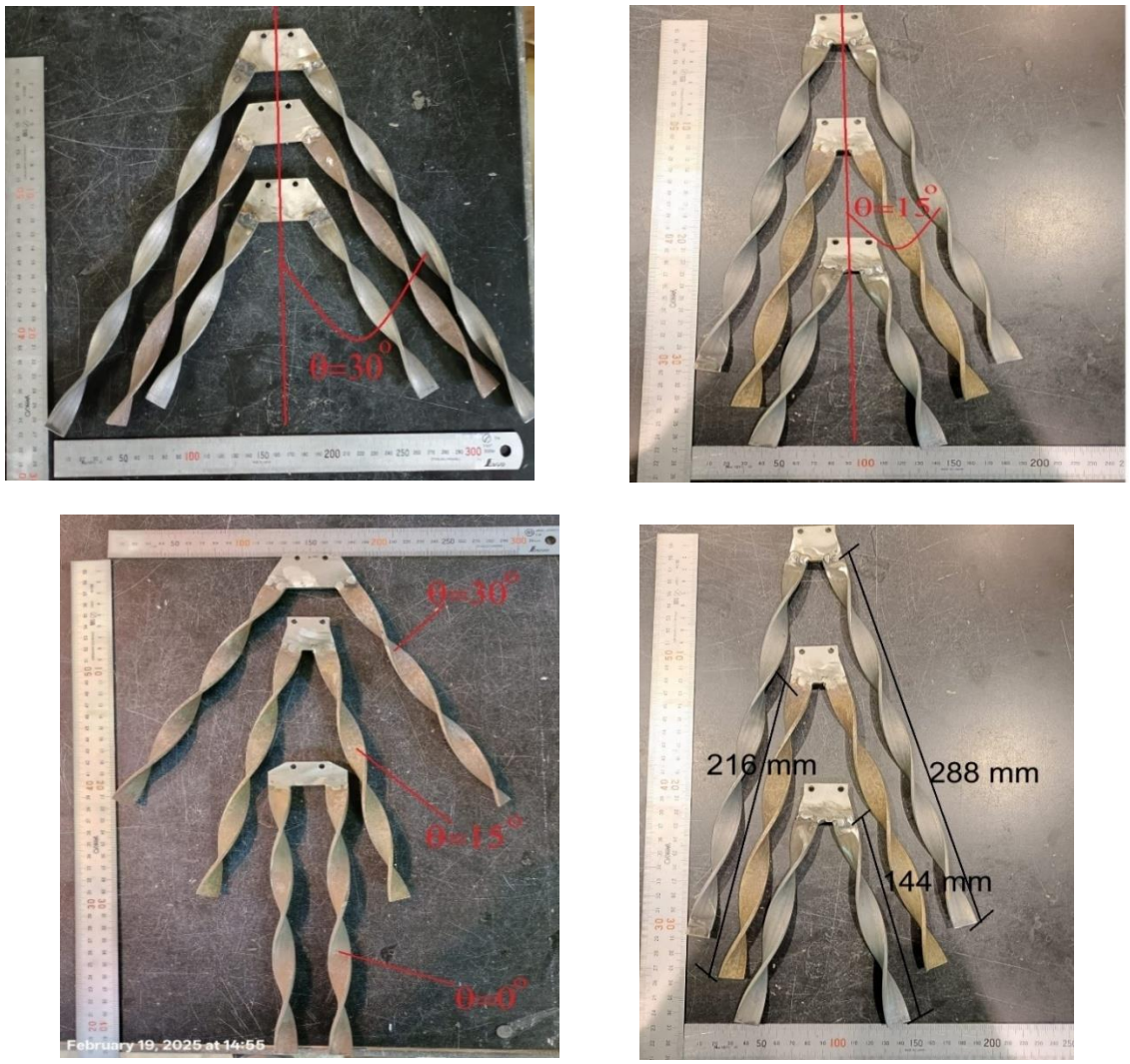

Figure 6. Grouped-pile models used in this study (configurations and dimensions) (Source: developed by the authors).

2.5 Explanation of the Scaling Law and Physical Modeling

As stated by [29], the first step in 1-g laboratory tests is to drive accurate scaling laws constitutes. Noting that every physical process can be expressed in terms of non-dimensional groups, the fundamental aspects of physics must be preserved in the design of the model tests. For cohesionless soil (sand), the stiffness parameter of the soil (i.e, the horizontal modulus subgrade reaction in this case) is roughly proportional to the square root of the depth below the ground surface (i.e, the vertical overburden pressure), as given in Eq. (3). The dimensionless group for the 1g test model in cohesionless soil can be considered as $\phi_1 = K_h L^{4.5/} E_p I_p$ (i.e, 4 for pile flexural stiffness plus 0.5 to account for the change in soil stiffness). This leads to the general scaling law for the pile load tests that are carried out in

granular soil, as given in the following equations:

$$K_h = n_h\sqrt{z} \quad (3)$$

$$(\phi_1)_m = \frac{n_h {L_m}^{4.5}}{E_m I_m} \quad (4)$$

$$(\phi_1)_p = \frac{n_h {L_p}^{4.5}}{E_p I_p} \quad (5)$$

$$\frac{(\phi_1)_p}{(\phi_1)_m} = \frac{L_p^{4.5}.I_m E_m}{L_m^{4.5}.I_p E_p} \quad (6)$$

$$\frac{E_m I_m}{E_p I_p} = \frac{L_m^{4.5}}{L_p^{4.5}} \quad (7)$$

$$\frac{L_m}{L_p} = \frac{1}{F} \quad (8)$$

$$\frac{E_m I_m}{E_p I_p} = \frac{1}{F^{4.5}} \quad (9)$$

where n_h is the coefficient of horizontal subgrade reaction of the soil; E_mI_m is the flexural rigidity of the model pile; E_pI_p is the flexural rigidity of the prototype pile; and F is the length scale factor, adopted as F = 10.

The relevant parameters for both the prototype and laboratory model piles are summarized in Table 3. Although the geostatic stress field does not fully replicate prototype-scale conditions, the pile's flexural rigidity was proportionally reduced to maintain similarity in structural response. Consequently, the physical modeling remains valid for studying soil–pile interaction. In this context, the relative stiffness ratio between the pile and the surrounding soil (E_p/E_s) was maintained constant throughout the tests to ensure representative behavior (almost equal to $30x10^3$).

Table 3. Equivalent values for the characteristics of the prototype and experimental model. (Source: compiled by the authors)

Parameter	Model	Prototype
Material	Steel	Cast iron
Modulus of elasticity of the pile material (E_p)	200 GPa	170 GPa
Flexural rigidity in the weak direction (EI_x)	0.0072 kN·m^2	227.68 kN·m^2
Flexural rigidity in the strong direction (EI_y)	0.2048 kN·m^2	6476.34 kN·m^2
Width of pile (B)	16 mm	250 mm
Thickness of the pile (t)	3 mm	40 mm
Load eccentricity (e)	0.05 m	0.75 m
Pile embedded length (L)	0.144, 0.216, and 0.288m	2.25, 3.40, and 4.50m
Scale factor	1	10

2.6 Definition of the Rigid and Flexible Piles

The relative stiffness factor K_{rs} was calculated for the pile models using the formula proposed by [30], as given in Eq. 10. For rigid piles, the value of K_{rs} is greater than ($1x10^{-2}$).

$$K = \frac{E_m I_m}{E_s L_s} \quad (10)$$

where: L= pile embedded length of pile.

The calculated values of (K_{rs}) for the pile models used in the experimental testing program were 0.071, 0.014, and 0.0044 for slenderness ratios (L/B) of 9, 13.5, and 18, respectively. Hence, the piles models are considered rigid piles for slenderness ratios of (L/B = 10 and 13.5), whereas it is considered flexible pile for slenderness ratio of (L/B = 18). Table 4 gives the values of the relative stiffness factors for all pile models.

Table 4. Calculations of the relative stiffness factors for all pile models. (Source: compiled by the authors)

L/B	L (mm)	E_mI_m (kN.m^2)	E_s (kPa)	K_{rs}	Pile type
9	144			0.071	Rigid
13.5	216	0.2	6500	0.014	Rigid
18	288			0.0044	Flexible

3. Test Procedures and Protocol

Table 5 summarizes the overall details of the testing program and the conditions for all conducted tests. The following procedures were implemented during the experimental campaign:

– Initially, the pile model was positioned at the center of the testing tank and clamped to a guide bar to minimize boundary effects.

– The soil was placed in successive, uniformly compacted layers of 10 cm thickness.

– After reaching the top level of the tank, the guide bar was removed, and the surface was leveled.

– Measurement devices (LVDTs) were installed on the test setup.

– A lateral cyclic load was applied to the pile head using a servo-hydraulic actuator. The loading sequence involved displacing the pile head forward by 2 mm, then laterally backward by 4 mm, and finally returning it to its initial position by 2 mm, as illustrated in Figure 4. Cyclic horizontal displacement was applied to the spiral pile group models for 100 to 200 cycles to investigate their long-term response under repeated loading.

Table 5. Experimental program overview and conditions of the tests. (Source: compiled by the authors)

No	Test ID	Pile arrangement/orientation pattern with respect to the lateral load direction	L/B	Batter angle (θ)	Loading characteristics
1	15-g spiral 144	2-piles group	9	30	Cyclic (N = 200), f (Hz) = 0.125 Hz

2	30-g spiral 144	(Two piles on series - one column of piles)			Cyclic (N = 200), f (Hz) = 0.125 Hz
3	30-g spiral 144			60	Cyclic (N = 200), f (Hz) = 0.075 Hz
4	30-g spiral 144				Cyclic (N = 200), f (Hz) = 0.025 Hz
5	0-g spiral 216			0	Cyclic (N = 200), f (Hz) = 0.075 Hz
6	15-g spiral 216			30	Cyclic (N = 200), f (Hz) = 0.125 Hz
7	30-g spiral 216		13.5		Cyclic (N = 200), f (Hz) = 0.125 Hz
8	30-g spiral 216			60	Cyclic (N = 200), f (Hz) = 0.075 Hz
9	30-g spiral 216				Cyclic (N = 200), f (Hz) = 0.025 Hz
10	0-g spiral 216			0	Cyclic (N = 200), f (Hz) = 0.075 Hz
11	15-g spiral 216	2-piles group (Two piles on parallel-one row of piles)		30	Cyclic (N = 200), f (Hz) = 0.125 Hz
12	30-g spiral 216		13.5		Cyclic (N = 200), f (Hz)= 0.125Hz
13	30-g spiral 216			60	Cyclic (N = 200), f (Hz)= 0.075Hz
14	30-g spiral 216				Cyclic (N = 200), f (Hz) = 0.025 Hz
15	30-g spiral 288			30	Cyclic (N = 200), f (Hz) = 0.125 Hz
16	30-g spiral 288	2-piles group (Two piles on series-one column of piles)	18		Cyclic (N = 200), f (Hz) = 0.125 Hz
17	30-g spiral 288			60	Cyclic (N = 200), f (Hz) = 0.075 Hz
18	30-g spiral 288				Cyclic (N = 200), f (Hz) = 0.025 Hz

Note:

It is significant to mention that in this study, the effect of the pile group arrangement with respect to the loading direction was also investigated. Hence, the grouped-piles of slenderness ratio of (L/B=13.5) were selected for being tested in two different arrangement patterns, including: case (I) two-piles on series (one row of piles), and case (II) two-piles on parallel (one column of piles), as shown in Figure 7a and Figure 7b, respectively.

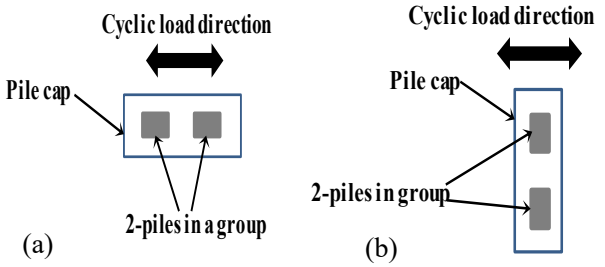

Figure 7. Grouped-pile arrangement: (a) two piles in series (one row of piles – Case I); (b) two piles in parallel (one column of piles – Case II) (Source: developed by the authors).

4. Results and Discussion

In the following sections, a comprehensive analysis of the results of the conducted tests has been presented.

4.1 Maximum Cyclic Lateral Load Resistance

The relationships between the measured cyclic lateral loads (H_{cyc}) and the number of loading cycles (N) along with the loading frequency (f) for the flexible and rigid grouped pile models after 100 cycles of lateral loading represented on a semi-log scale are shown in Figure 8.

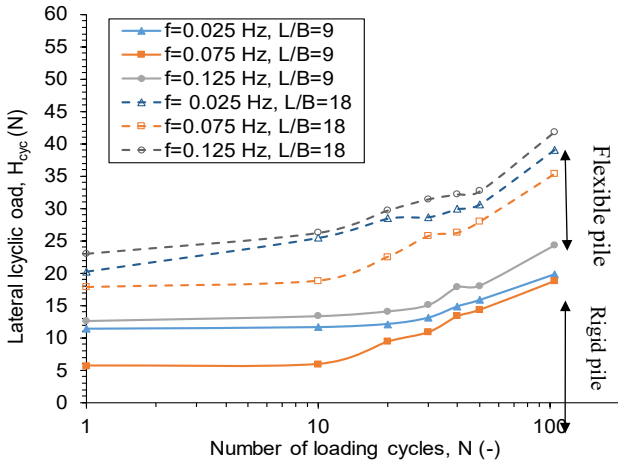

Figure 8. Variation of the measured cyclic lateral loads (H_{cyc}) versus the number of loading cycles (N) along with the loading frequency (f) for the flexible and rigid grouped piles of batter angel =30°). (Source: developed by the authors)

The results show that the lateral cyclic resistance of pile groups increases significantly with the number of load cycles (N), slenderness ratio (L/B), and loading frequency (f), following nonlinear trends. Furthermore, flexible pile groups exhibit notably higher lateral resistance compared to stiffer configurations. This

behavior clearly indicates a substantial change in the soil stress state due to evolving soil–pile interaction mechanisms under repeated lateral loading.

Furthermore, Figures 9 and 10 illustrate the influence of the number of lateral cyclic load applications (N) and batter angles (θ) on the response of pile groups for rigid (L/B = 9) and flexible (L/B = 18) configurations, respectively. The variation of the measured cyclic lateral load (H_cyc) with the number of loading cycles (N) indicates that both flexible and rigid pile groups are significantly affected by the accumulation of cyclic loading.

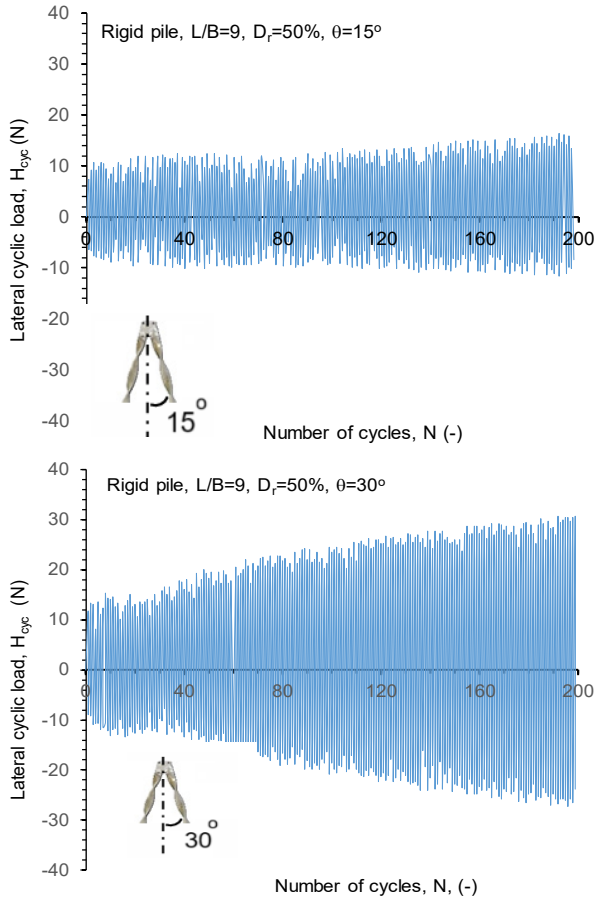

Figure 9. Variation of cyclic lateral pile resistance with the number of cycles for rigid grouped piles (L/B = 9) after 200 cycles (Source: developed by the authors)

In terms of lateral resistance, the results show that, regardless of the slenderness ratio (L/B), pile groups with a batter angle of 30° exhibit nonlinear load-displacement behavior. In contrast, pile groups with a batter angle of 15° demonstrate predominantly linear behavior under the applied loading conditions.

4.2 Hysteretic performance

Figures 11, 12 and 13 illustrate the results of normalized hysteretic lateral cyclic load-displacement curves for flexible and rigid grouped-piles of slenderness ratios (L/B) equal to 18, 13.5 and 9, respectively, after applying 200 cycles (N) of lateral loading.

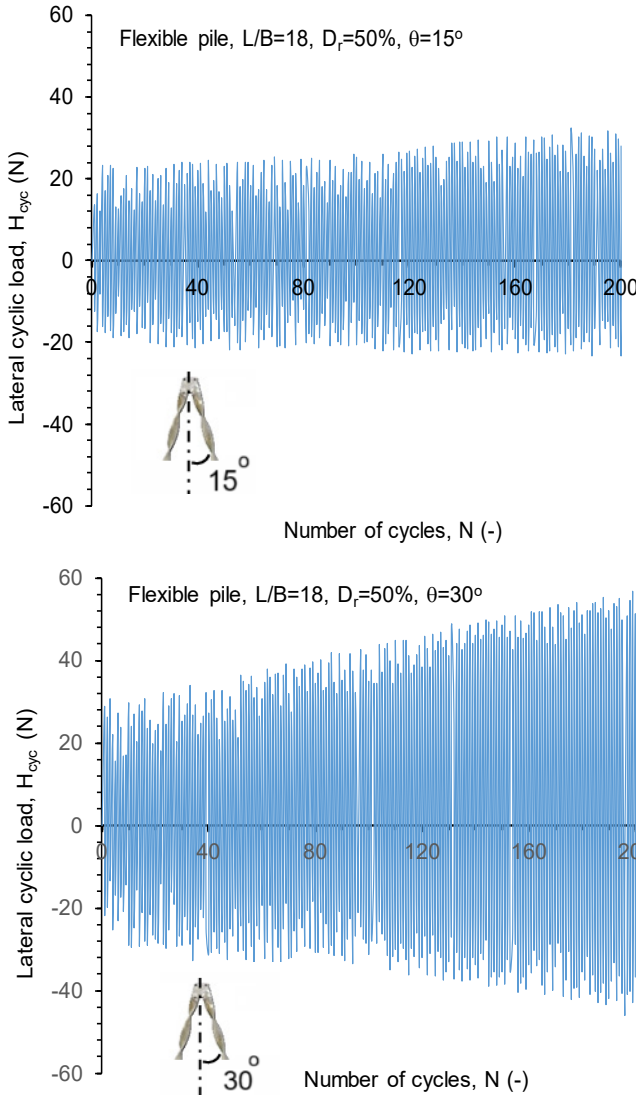

Figure 10. Variation of cyclic lateral pile resistance with the number of cycles for flexible grouped piles (L/B = 18) after 200 cycles (Source: developed by the authors)

In the shown normalized hysteretic loop curves, the vertical axis represents the measured cyclic lateral loads (H_{cyc}) which were normalized with respect to the maximum lateral cyclic load (H_{max}) measured at the end of cyclic test (N=200 loading cycles). The horizontal axis represents the measured pile head lateral displacements (y), which were normalized with respect to the maximum lateral displacement (y_{max}) (i.e, equal 20% of pile width, 0.2B = 3.2mm).

It can be seen that for the flexible grouped pile (Figure 11), the enclosed areas of the generated hysteretic loop curves are much smaller (narrower) compared to those curves generated in the rigid piles (Figures 12 and 13).

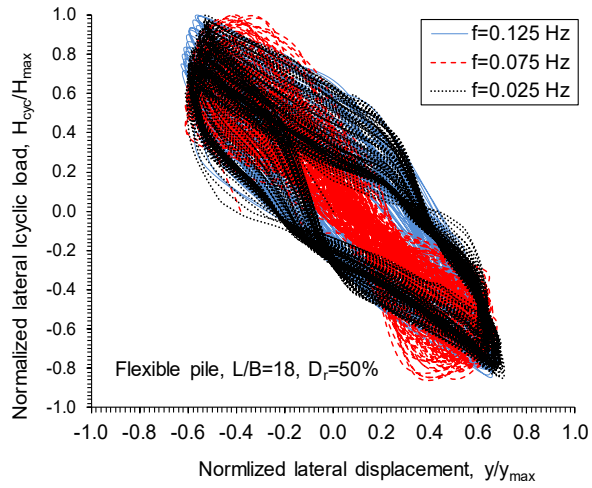

Figure 11. Normalized hysteretic lateral load-displacement curves for grouped piles of slenderness ratio (L/B) = 18 (Source: developed by the authors)

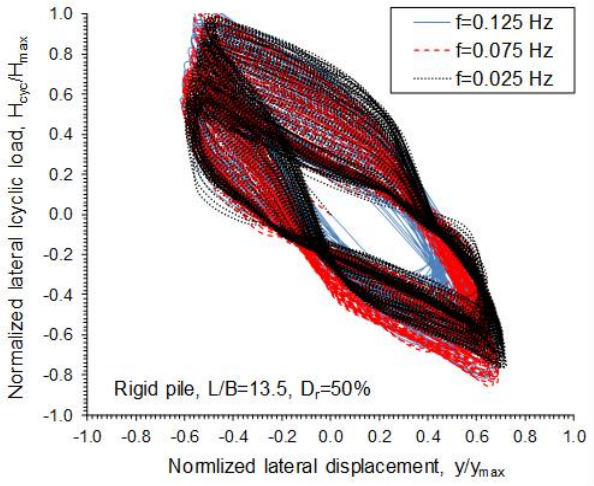

Figure 12. Normalized hysteretic lateral load-displacement curves for grouped piles of slenderness ratio (L/B) = 13.5 (Source: developed by the authors)

Overall, the hysteretic loops of all the tests showed nonlinearity trends and experienced quite a change in the response of the grouped pile by alternating the slenderness ratio (L/B). However, the loading frequency (f) showed a minor effect on the generated hysteresis curves as all loop curves were mostly coincident with each other.

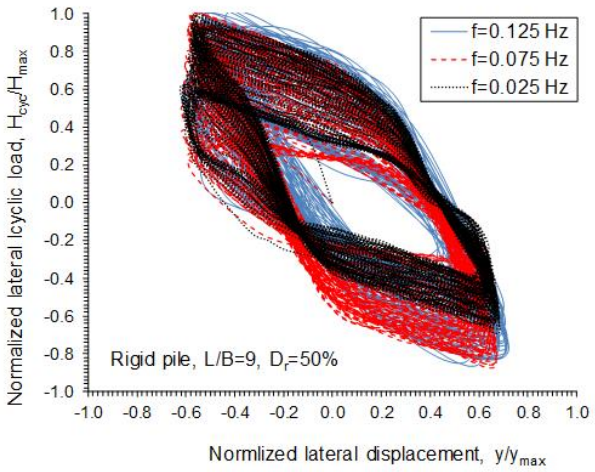

Figure 13. Normalized hysteretic lateral load-displacement curves for grouped piles of slenderness ratio (L/B) = 9. (Source: developed by the authors).

4.3 Influence of Loading Frequency and Pile Batter Angle on Lateral Resistance of Pile Groups

In this experimental study, grouped pile models were subjected to lateral cyclic loading across a range of frequencies (f) from 0.075 Hz to 0.125 Hz. Figure 14 presents the effects of varying loading frequency (f) and slenderness ratio (L/B) on the maximum lateral load capacity of the pile groups after 200 cycles.

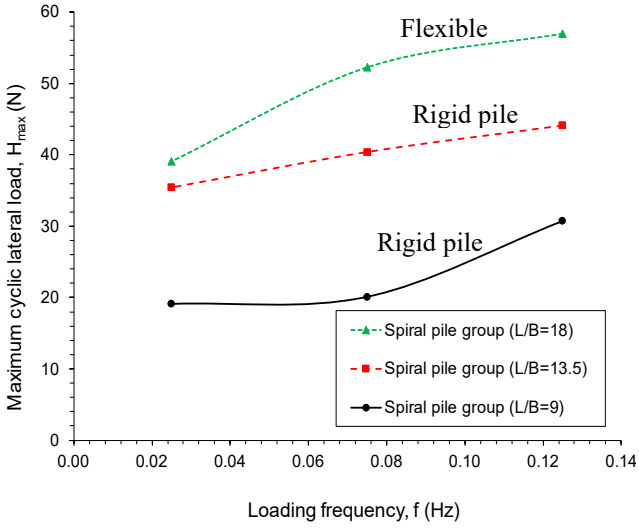

Figure 14. Effect of the loading frequency and slenderness ratio on the lateral capacities of the pile groups after 200 cycles of lateral loading (Source: developed by the authors)

The results show that increasing both the loading frequency and slenderness ratio leads to enhanced pile–soil interaction, resulting in higher system stiffness and improved lateral load resistance. This behavior is attributed to the progressive densification of the soil within the pile group, driven by an increased rate of lateral loading. The rise in confining stresses due to rapid cyclic straining contributes to greater soil restraint

and, consequently, improved overall performance of the foundation system.

4.4 Influence of the Grouped-Pile Arrangement and Orientation

4.4.1 Maximum Lateral Cyclic Loads of the Grouped Piles

As previously stated, the influence of pile group configuration on the maximum lateral cyclic load capacity was investigated using a grouped-pile model with a slenderness ratio of L/B = 13.5 under two distinct loading conditions.

In the first case, the two-pile group was arranged in series (i.e, a single row) relative to the direction of lateral loading (see Figure 7a). In the second case, the group was configured in parallel (i.e, a single column) with respect to the lateral loading direction (see Figure 7b).

Figure 15 illustrates the relationship between the maximum measured lateral cyclic load (H_{max}) and pile batter angle (θ) for the two group configurations. For the parallel arrangement (i.e, a single column of piles), increasing the batter angle has negligible effect on lateral load capacity, with minimal variation in the group's lateral resistance. In contrast, for the series arrangement (i.e, a single row of piles), the lateral resistance increases significantly with higher batter angles (θ). This behavior can be attributed to the soil confined between the pile shafts, which undergoes repeated cycles of in-plane shear stresses under lateral loading. This cyclic straining promotes progressive soil densification, thereby enhancing the overall stiffness and load-bearing capacity of the group.

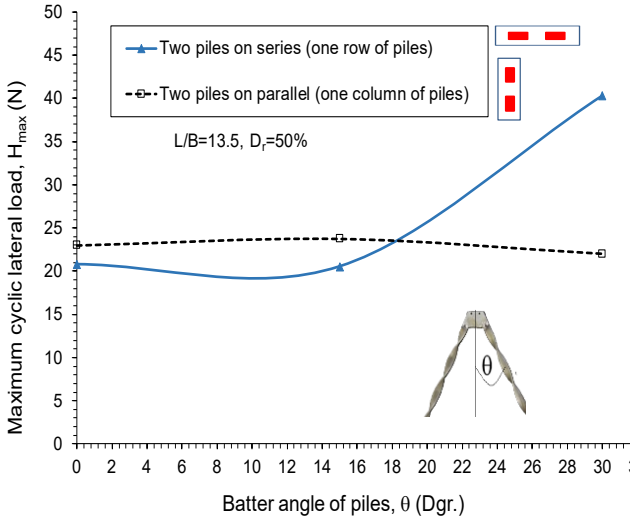

Figure 15. Relationships between the batter angle of the pile group and the maximum measured lateral cyclic loading for the pile group with a slenderness ratio =13.5 (Source: developed by the authors)

4.4.2 Vertical Displacement of the Grouped Piles

In the present 1-g model tests, vertical displacements of the pile group models were monitored using attached linear variable differential transformers (LVDTs). Upward vertical deformations (S_v) were observed in the pile groups under repeated lateral cyclic loading. These vertical movements were measured for two pile group configurations relative to the direction of lateral loading: (i) piles arranged in series (single row), and (ii) piles arranged in parallel (single column).

Figure 16 presents the variation of vertical displacement with the number of load cycles (N) for pile groups with a slenderness ratio of L/B = 13.5 in the series arrangement. The results indicate that significant upward vertical movements occurred in battered pile groups (θ = 15° and 30°) as the number of cycles increased. In contrast, a substantial reduction in upward displacement was observed when the piles were installed vertically (θ = 0°). This demonstrates that both in-plane shear mechanisms and pile batter angle (θ) significantly influence the response of laterally loaded pile groups.

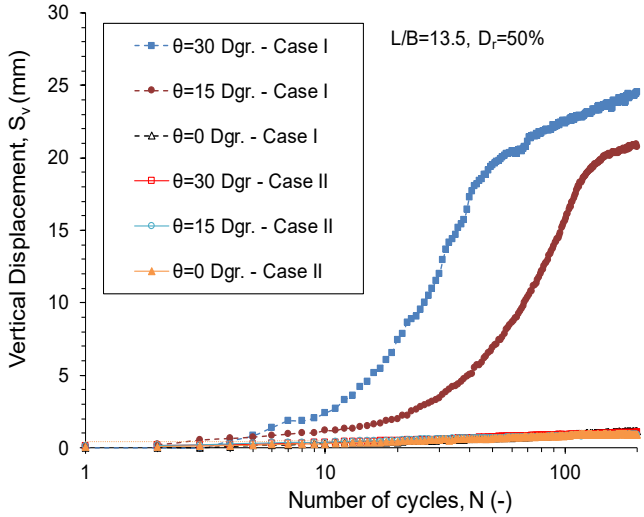

Figure 16. Variation of the vertical displacement with the number of cycles for 2-piles on series (one row of piles, Case I) and in parallel (one column of piles, Case II) (Source: developed by the authors)

In contrast, for the pile group arrangement with piles configured in parallel (i.e, a single column), a significant reduction in vertical upward displacement was observed across all batter angles (θ), compared to the series arrangement. This indicates that the batter angle has minimal influence on the response of laterally loaded pile groups in this configuration. The reduced vertical movement can be attributed to the fact that the lateral cyclic loading is applied out-of-plane relative to the group axis, resulting in negligible in-plane soil shearing within the pile group. Consequently, no significant shear zones develop between the piles, leading to more restrained vertical uplift and a stiffer overall response.

Likewise, Figure 17 presents the relationship between the number of load cycles (N) and the measured vertical displacement (S_v) for battered pile groups with batter angles of 15° and 30°.

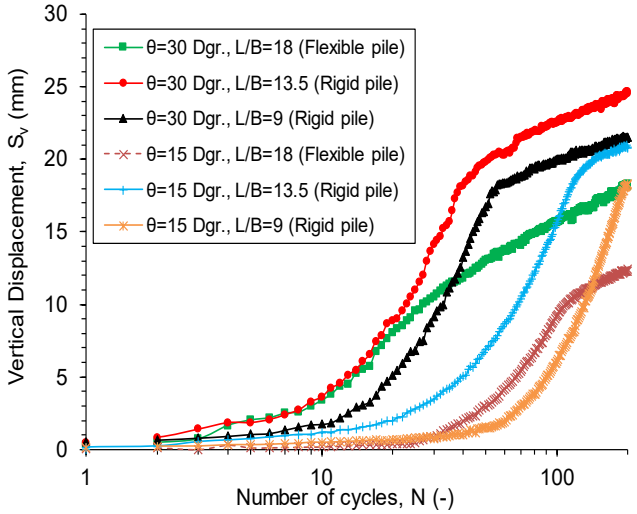

Figure 17. Variation of the vertical displacement with the number of cycles for the pile group of 2-piles of batter angle θ=30º and 15º installed in medium dense sand soil (Source: developed by the authors)

The results demonstrate that upward vertical displacement increases with larger batter angles. The pile group was arranged in series (i.e, a single row) relative to the direction of lateral loading.

As shown in Figure 17, the maximum upward displacements were 18.31 mm, 24.50 mm, and 21.50 mm for pile groups with slenderness ratios (L/B) of 18, 13.5, and 9, respectively. However, there appears to be an inconsistency in the text: the second sentence repeats similar values (11.31 mm, 20.74 mm, and 18.27 mm) without clarifying the corresponding conditions (e.g, different batter angle or configuration). If these values refer to a different test condition (e.g, θ = 15°), this should be explicitly stated.

Table 6 summarizes the measured upward vertical movements for all tested configurations. The phenomenon of upward pile displacement is further discussed and analyzed in detail in the following section.

Table 6. Maximum measured values of vertical displacements for grouped piles after 200 cycles of loadings (Source: compiled by the authors)

Grouped-pile arrangement	Slenderness ratio (L/B)	Batter angle (θ), Dgr.		
		0º	15º	30º
2-piles group (Two piles on parallel - one row of piles)	18	NA	NA	NA
	13.5	1.15mm	20.74mm	24.5mm
	9	NA	NA	NA
2-piles group (Two piles on series - one column of piles)	18	NA	12.32mm	18.31mm
	13.5	0.91mm	0.92mm	1.06mm
	9	NA	18.27mm	21.50mm

4.5 Discussion on the Soil Rocking Phenomenon

In the previous analysis of the vertical displacement results, it was noticed that the vertical upward movements for the grouped piles were measured by increasing the number of loading cycles (N) and batter angles (θ) of pile models. This phenomenon was revealed because of rocking of soil particles under the effect of external repeated lateral cyclic which acted on grouped-piles when the piles were set on series arrangement. Repeated lateral cyclic loads resulted in an increase in the vertical overburden pressure due to the shaking of the dry sand. Therefore, this motion can cause serious risks to the integrity of a structure and is important to understand in the context of geotechnical engineering and construction.

As shown in Figure 18, during cyclic lateral loading on grouped piles of two piles in series (one row of piles), the forces on the piles have simultaneously changed in the following pattern. The trialing pile is subjected to a combined loading condition of compression and lateral loads, whereas the leading pile is subjected to a combined loading condition of uplift and lateral loads.

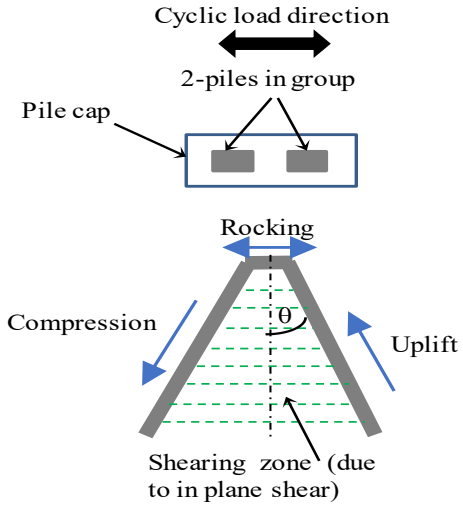

Figure 18. Load distribution and rocking action created in 2-piles on series group (one row of piles) (Source: developed by the authors)

Consequently, as this action occurs periodically throughout the lateral loading, shearing zones (in-plane shear) are gradually created between the trailing and leading pile walls inside the group. This loading

condition results in the upward movement of grouped piles and rocking of the soil so that the overall instability of the foundations occurs.

On the other hand, during cyclic lateral loading on grouped piles of two piles in parallel (one column of piles), the imposed lateral cyclic force is evenly distributed over the two piles in the horizontal direction, causing equal load sharing between the two piles in the pure lateral direction, as shown in Figure 19. Accordingly, out-of-plane shear stresses are generated outside of the pile group, and the pile-soil interaction extremely diminishes; no foundation rocking phenomenon occurred in this case of the pile group arrangement.

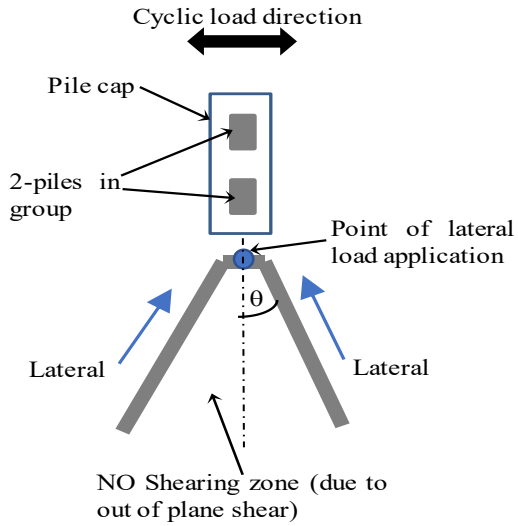

Figure 19. Load distribution in 2-piles on parallel group (one column of piles) (Source: developed by the authors)

5. Conclusion

This paper presents the results of an experimental study conducted using 1-g physical modeling to investigate the behavior of steel spiral pile group foundations that are commonly used to support onshore renewable energy structures under lateral cyclic loading. The stability of the pile groups, in terms of lateral resistance and vertical displacement, was systematically evaluated. The following conclusions are drawn:

1. Lateral resistance of pile groups increases significantly with the number of load cycles (N), slenderness ratio (L/B), and loading frequency (f). This enhancement is attributed to soil densification caused by the repeated straining and variation in the rate of loading, which improves soil-pile interaction and system stiffness.

2. For pile groups arranged in parallel (i.e, a single column), increasing the batter angle (θ) has negligible effect on lateral resistance. This is because lateral loading acts out-of-plane relative to the group axis, resulting in minimal in-plane soil shearing between the piles.

3. In contrast, for pile groups arranged in series (i.e, a single row), lateral resistance increases with larger batter angles (θ). The soil confined between the leading and trailing piles is subjected to successive cycles of in-plane shear stresses, promoting the development of localized shear zones and enhancing overall group performance.

4. Under repeated in-plane lateral loading, a phenomenon of soil "rocking" was observed around the pile group. This mechanism induces upward vertical displacement and represents a critical condition that may compromise foundation stability. Therefore, it must be considered in the design process to ensure structural safety. These findings highlight the importance of pile orientation and group configuration in optimizing the performance of steel spiral pile foundations and should be incorporated into engineering practice during installation.

It is worth noting that the conclusions presented above are based on 1-g laboratory tests conducted at a small scale. Caution should be exercised when applying these results to different testing conditions or full-scale field applications. Nevertheless, the findings provide valuable preliminary insights and serve as a reliable reference for validating numerical models and guiding future studies involving centrifuge testing or full-scale experiments on spiral pile foundations for renewable energy structures.

Declarations

Author Contributions

Conceptualization, M.A, R.I. and T.K.; methodology, M.A, and T.K; experimental work and testing, A.A, and M.A; formal analysis of results, M.A, A.A, and R.I.; investigation, M.A, and T.K.; resources, R.I, A.A, and T.K.; data curation, M.A.; writing—original draft preparation, all authors contributed equally; writing—review and editing, A.A, M.A. and R.I.; visualization, M.A.; supervision, R.I.; All authors have read and agreed to the published version of the manuscript.

Data Availability Statement

The data presented in this study are available on request from the corresponding author.

Funding

Funding information is not available.

Acknowledgements

The authors would like to sincerely thank HINODE Holdings Co. Ltd and the geotechnical engineering laboratory at Kyushu University, which provided the experimental materials during this research. The first author gratefully acknowledges the support provided by

The Ministry of Higher Education and Scientific Research of Egypt (MHESR) and The Japan International Cooperation Agency (JICA) during the research visit to Kyushu University.

Institutional Review Board Statement

Not applicable.

Conflicts of Interest

The author declares that there are no conflicts of interest regarding the publication of this manuscript.

References

[1] ARANY L, BHATTACHARYA S, MACDONALD J, and HOGAN S.J. Simplified critical mudline bending moment spectra of offshore wind turbine support structures. *Wind Energy*, 2014, 18: 2171-2197. https://doi.org/10.1002/we.1812

[2] TAMBOURA H, YAMAUCHI R, and ISOBE K. Bearing capacity evaluation of small-diameter spiral piles in soft ground subjected to combined loads. *Soils and Foundations*, 2022, 62(5): 1–15. https://doi.org/10.1016/j.sandf.2022.101204

[3] KANG S, JEONGDU N. and JANG H. Support characteristics of eco-spiral pile with respect to twisting angle and ratio of borehole diameter to pile width. *International Journal of Mining, Reclamation and Environment*, 2019, 33(4), 265-285, https://doi.org/10.1080/17480930.2017.1399007

[4] WANG X, LI S, and LI J. Effect of pile arrangement on lateral response of group-pile foundation for offshore wind turbines in sand. *Applied Ocean Research*, 2022, 124: 103194. https://doi.org/10.1016/j.apor.2022.103194

[5] OHNISHI N, and NISHIOKA H. Experimental study on the pile group effect in the horizontal resistance of spiral piles. Proceeding of the 2nd International Conference on Press-in Engineering 2021, Kochi, Japan – Matsumoto et al (eds), Taylor & Francis Group, London, pp. 203-209. https://doi.org/10.1201/9781003215226-16

[6] KUROKAWA T, TANI Y, NAGATA M, JUGDERNAMJIL A, and YASUFUKU N. A study on analysis of horizontal resistance of screw coupled foundation with vertical and battered piles in cohesionless soil. *Proceeding of the 2nd International Confrence on Press-in Engineering*, 2021, Kochi, Japan. Matsumoto et al (eds), Taylor & Francis Group, London, pp. 224-234. https://doi.org/10.1201/9781003215226-19

[7] DING H, WANG L, ZHANG P, LIANG Y, TIAN Y. and QI X. The recycling torque of a single-plate helical pile for offshore wind turbines in dense sand. *Applies Sciences*, 2019, 9(19): 4105, https://doi.org/10.3390/app9194105.

[8] PERKO H A. *Helical piles. A practical guide to design and installation*, 1st edn. Hoboken, NJ, USA: John Wiley & Sons, 2009.

[9] ROSQUOET F, THOREL L, GARNIER J, and CANEPA Y. Lateral cyclic loading of sand-installed piles. *Soils and Foundations*, 2007, 47(5): 821–832. https://doi.org/10.3208/sandf.47.821

[10] LONG J, and VANNESTE G. Effects of cyclic lateral loads on piles in sand. *ASCE Journal of Geotechnical Engineering*, 1994, 120(1): 225–243. https://doi.org/10.1061/(ASCE)0733-9410(1994)120:1(225)

[11] LIN S, and LIAO J. Permanent strains of piles in sand due to cyclic lateral loads. *Journal of Geotechnical and Geo-environmental Engineering*, 1999, 125(9): 798–802. https://doi.org/10.1061/(ASCE)1090-0241(1999)125:9(798)

[12] LITTLE R, and BRIAUD L. Full scale cyclic lateral load tests on six single piles in sand. Miscellaneous Paper GL-88-27, Geotechnical Division, Texas A&M University, College Station, Texas, 1988.

[13] HETTLER A. Displacements of rigid and elastic foundation body in the sand at monotonic and cyclic loading. PhD thesis, Department of Civil Engineering, Geo- and Environmental Sciences, Institute of Soil Mechanics and Rock Mechanics, University of Karlsruhe, 1981.

[14] AWAD-ALLAH F, YASUFUKU N, and ABDEL-RAHMAN A. Cyclic response of wind turbine on piles in unsaturated sand. *International Journal of Physical Modelling in Geotechnics*, 2017, 17(3): 161-176. https://doi.org/10.1680/jphmg.15.00017

[15] ACHMUS M, KUO Y, and ABDEL-RAHMAN K. Behavior of mono-pile foundations under cyclic lateral load. *Computers and Geotechnics*, 2009, 36(5): 725–735. https://doi.org/10.1016/j.compgeo.2008.12.003

[16] HIRATA A, KOKAJI S, KANG S, and GOTO T. Study on the estimation of axial resistance of spiral bar based on interaction with ground. *Journal of the Mining and Materials Processing Institute of Japan (Shigen-Sozai)*, 2005, 121 (8): 370-377. https://doi.org/10.2473/shigentosozai.121.370 (in Japanese).

[17] SAHIL A, UCHIMURA T, MALIK and KABIR Md A comparative study on the end-bearing capacity of toe-wing and spiral screw piles in cohesionless soil. *Buildings*, 2025, 15(4): 525 https://doi.org/10.3390/buildings15040525

[18] KUROKAWA T, IDE Y, YASUFUKU N, and NAGATA M. Horizontal resistance characteristics of batter-coupled spiral piles under monotonic and cyclic loading. *Lowland Technology International*, 2024; 24(4): 1-12. https://doi.org/10.0001/ialt_lti.v24i4.1711

[19] JUGDERNAMJIL A, YASUFUKU N and ALOWAISY A. Prediction of ultimate lateral capacity of rigid spiral pile under static loading in cohesionless soil. *Lowland Technology International*, 2021, 23(3), 17-28. https://doi.org/10.0001/ialt_lti.v23i3.1074

[20] SATO T, OTANI J, CHEVALIER B, and ESKISAR T. Effect of shaft rotation of driven spiral piles on vertical bearing capacity. *The 15th Asian Regional Conference on Soil Mechanics and Geotechnical Engineering, Japanese Geotechnical Society Special Publication*, 2016, 2(36): 1304-1309. https://doi.org/10.3208/jgssp.JPN-110.

[21] O'NEILL M, and MURCHISON M. An evaluation of p-y relationships in sands. Report (American Petroleum Institute), PRAC 82-41-1, Research report (University of Houston. Department of Civil Engineering), GT-DF02-83, 1983.

[22] CHANDRASEKARAN S, BOOMINATHAN A, and DODAGOUDAR R. Experimental investigations on the behavior of pile groups in clay under lateral cyclic loading. *Geotechnical and Geological Engineering*, 2010, 28(5): 603–617. https://doi.org/10.1007/s10706-010-9318-4

[23] LEBLANC C, BYRNE B.W, and HOULSBY G.T. Response of stiff piles in sand to long term cyclic loading. *Geotechnique*, 2010, 60(2): 79–90. https://doi.org/10.1680/geot.7.00196

[24] MIURA S, and TOKI S. A simple preparation

method and its effect on static and dynamic deformation-strength properties of sand. *Soils and Foundations*, 1982, 22(1): 61–77. https://doi.org/10.3208/SANDF1972.22.61
[25] JAPANESE GEOTECHNICAL SOCIETY. JGS 1431: Portable cone penetration test, 2003. (In Japanese).
[26] NIKUDEL M R, MOUSAVI S E, KHAMEHCHIYAN M, and JAMSHIDI A. Using miniature cone penetration test (Mini-CPT) to determine engineering properties of sandy soils. *Journal of Geopersia*, 2012, 2(2): 65–76. https://doi.org/10.22059/jgeope.2012.29232
[27] LOMBARDI D, BHATTACHARYA S, SCARPA FABRIZIO and BIANCHI M. Dynamic response of a geotechnical rigid model container with absorbing boundaries. *Soil Dynamics and Earthquake Engineering*, 2015, 69: 46–56. https://doi.org/10.1016/j.soildyn.2014.09.008
[28] BASACK S, and PURKAYASTHAB D. Behavior of single pile under lateral cyclic load in marine clay. *Asian Journal of Civil Engineering*, 2007, 8(4): 443–458. https://ajce.bhrc.ac.ir/Portals/25/PropertyAgent/2905/Files/6233/443.pdf
[29] WOOD D M, CREWE A, and TAYLOR C. Shaking table testing of geotechnical models. *International Journal of Physical Modeling in Geotechnics*, 2002, 2(1): 1–13. https://doi.org/10.1680/ijpmg.2002.020101
[30] POULOS H G, and DAVIS E H. *Pile foundation analysis and design*. John Wiley & Sons, New York, 1980.

参考文:

[1] ARANY L, BHATTACHARYA S, MACDONALD J, 和 HOGAN S.J.海上风力涡轮机支撑结构的简化临界泥线弯矩谱。《风能》，2014, 18: 2171-2197。https://doi.org/10.1002/we.1812
[2] TAMBOURA H, YAMAUCHI R, 和 ISOBE K. 软土地基中小直径螺旋桩在组合荷载作用下的承载力评估。《土壤与地基》，2022, 62(5): 1-15。https://doi.org/10.1016/j.sandf.2022.101204。
[3] KANG S, JEONGDU N. 和 JANG H. 生态螺旋桩支护特性随扭转角和钻孔径桩比变化的关系.《国际采矿、复垦与环境杂志》2017，33(4)，265-285，https://doi.org/10.1080/17480930.2017.1399007。
[4] WANG X, LI S 和 LI J 桩基布置对沙地海上风电群桩基础横向响应的影响。《应用海洋研究》, 2022, 124: 文章 103194。https://doi.org/10.1016/j.apor.2022.103194。
[5] OHNISHI N 和 NISHIOKA H 桩群效应对螺旋桩水平阻力影响的试验研究。第二届国际压入工程会议论文集，2021 年，日本高知 – Matsumoto 等编，Taylor & Francis 集团，伦敦，第 203-209 页。https://doi.org/10.1201/9781003215226-16。
[6] KUROKAWA T、TANI Y、NAGATA M、JUGDERNAMJIL A 和 YASUFUKU N。无粘性土中带垂直桩和斜桩的螺旋耦合基础水平阻力分析研究。第二届国际压入工程会议论文集，2021，日本高知。Matsumoto 等编，泰勒·弗朗西斯集团，伦敦，第 224-234 页。https://doi.org/10.1201/9781003215226-19
[7] DING H, WANG L, ZHANG P, LIANG Y, TIAN Y. 和 QI X. 密实砂土中海上风力涡轮机单板螺旋桩的循环扭矩。《应用科学》，2019，9(19): 4105，https://doi.org/10.3390/app9194105。
[8] PERKO H A. 螺旋桩。设计和安装实用指南，第一版。美国新泽西州霍博肯：约翰·威利父子公司，2009。
[9] ROSQUOET F, THOREL L, GARNIER J 和 CANEPA Y. 砂土桩的横向循环荷载。土工与地基，2007，47(5): 821–832。https://doi.org/10.3208/sandf.47.821
[10] LONG J 和 VANNESTE G. 循环横向荷载对砂土中桩的影响。ASCE 岩土工程杂志，1994，120(1): 225–243。https://doi.org/10.1061/(ASCE)0733-9410(1994)120:1(225)
[11] LIN S 和 LIAO J. 循环横向荷载作用下砂土中桩的永久应变。岩土与土工环境工程杂志，1999，125(9): 798–802。https://doi.org/10.1061/(ASCE)1090-0241(1999)125:9(798)
[12] LITTLE R 和 BRIAUD L. 砂土中六根单桩全尺寸循环横向荷载试验。杂项论文 GL-88-27，德克萨斯农工大学岩土工程系，德克萨斯州学院站，1988。
[13] HETTLER A. 单调和循环荷载作用下砂土中刚性和弹性地基体的位移。博士论文，土木工程、地质与环境科学系，土力学与岩石力学研究所，卡尔斯鲁厄大学，1981。
[14] AWAD-ALLAH F、YASUFUKU N 和 ABDEL-RAHMAN A. 非饱和砂土中风力涡轮机对桩基的循环响应。国际岩土工程物理建模杂志，2017，17(3): 161-176。https://doi.org/10.1680/jphmg.15.00017
[15] ACHMUS M、KUO Y 和 ABDEL-RAHMAN K. 单桩基础在循环横向荷载作用下的性能。计算机与岩土工程，2009，36(5): 725–735。https://doi.org/10.1016/j.compgeo.2008.12.003
[16] HIRATA A、KOKAJI S、KANG S 和 GOTO T. 基于与地面相互作用的螺旋筋轴向阻力估算研究。日本矿业与材料加工协会期刊（Shigen-Sozai），2005，121 (8): 370-377。https://doi.org/10.2473/shigentosozai.121.370（日文）。
[17] SAHIL A、UCHIMURA T、MALIK 和 KABIR Md. 无粘性土中翼尖桩和螺旋桩端部承载力比较研究。《建筑》，2025，15(4): 525 https://doi.org/10.3390/buildings15040525
[18] KUROKAWA T、IDE Y、YASUFUKU N 和

NAGATA M. 单调和循环荷载下斜接螺旋桩的水平阻力特性。《低地技术国际》，2024； 24(4): 1-12。https://doi.org/10.0001/ialt_lti.v24i4.1711

[19] JUGDERNAMJIL A, YASUFUKU N 和 ALOWAISY A. 无黏性土中静态荷载作用下刚性螺旋桩极限横向承载力预测。低地技术国际公司，2021，23(3)，17-28。https://doi.org/10.0001/ialt_lti.v23i3.1074

[20] SATO T, OTANI J, CHEVALIER B 和 ESKISAR T. 打入螺旋桩桩身旋转对竖向承载力的影响。第 15 届亚洲土力学与岩土工程区域会议，日本岩土工程学会特刊，2016，2(36): 1304-1309。https://doi.org/10.3208/jgssp.JPN-110。

[21] O'NEILL M 和 MURCHISON M. 砂土中 p-y 关系的评估。报告（美国石油学会），PRAC 82-41-1，研究报告（休斯顿大学土木工程系），GT-DF02-83，1983。

[22] CHANDRASEKARAN S、BOOMINATHAN A 和 DODAGOUDAR R. 横向循环荷载作用下黏土中群桩行为的试验研究。岩土与地质工程，2010，28(5): 603–617。https://doi.org/10.1007/s10706-010-9318-4

[23] LEBLANC C、BYRNE B W, 和 HOULSBY G.T. 砂土中硬桩对长期循环荷载的响应。岩土技术，2010，60(2): 79–90。https://doi.org/10.1680/geot.7.00196

[24] MIURA S 和 TOKI S. 一种简单的制备方法及其对砂土静态和动态变形强度特性的影响。土工与地基，1982，22(1): 61–77。https://doi.org/10.3208/SANDF1972.22.61

[25] 日本岩土工程学会。JGS 1431：便携式静力触探试验，2003。（日文）。

[26] NIKUDEL M R、MOUSAVI S E、KHAMEHCHIYAN M 和 JAMSHIDI A. 利用微型静力触探试验（Mini-CPT）确定砂土的工程特性。吉奥波斯杂志，2012，2(2): 65–76 https://doi.org/10.22059/jgeope.2012.29232

[27] LOMBARDI D、BHATTACHARYA S、SCARPA FABRIZIO 和 BIANCHI M. 含吸收边界的土工刚性模型容器的动态响应。土动力学与地震工程，2015，69: 46–56。https://doi.org/10.1016/j.soildyn.2014.09.008

[28] BASACK S 和 PURKAYASTHAB D. 海洋粘土中单桩在横向循环荷载作用下的性能。亚洲土木工程杂志，2007，8(4): 443–458。https://ajce.bhrc.ac.ir/Portals/25/PropertyAgent/2905/Files/6233/443.pdf

[29] WOOD D M、CREWE A 和 TAYLOR C. 岩土模型振动台试验。《国际岩土物理建模杂志》，2002，2(1): 1-13。https://doi.org/10.1680/ijpmg.2002.020101

[30] POULOS H G 和 DAVIS E H. 桩基分析与设计。约翰·威利父子公司，纽约，1980。

Word count (excluding references): 9,233 words.

Peer-review record:

- ***Fast-track status:*** Not fast-tracked
- ***First-round reviews received:*** 3 reports
- ***Revision cycles completed:*** 3 rounds
- ***Final version submitted:*** July 17, 2025